Experimental Realization of Cavity Enhanced Spectroscopy on ^{88}Sr

Bachelor Thesis

By

Hans Chr. Stærkind

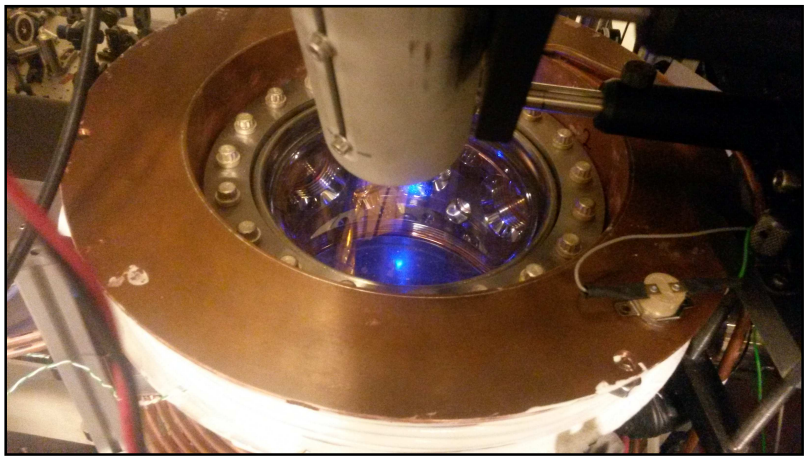

Under the supervision of Jan W. Thomsen

University of Copenhagen

Niels Bohr Institute

March 2014

Abstract

The purpose of this thesis is to review the physics of cavity enhanced spectroscopy, and introduce the cavity-atom system as a mean of stabilizing an optical atomic clock. The first part of the thesis is dedicated the experimental considerations on cooling a sample of atomic ^{88}Sr, and trapping it between two cavity mirrors. This involves Zeeman slowing, and magneto optical trapping. The second part outlines the basic theory and experimental methods necessary to turn the cavity-atom system into a stabilizing mechanism for an optical clock. The NICE-OHMS technique plays a central role here. The experimental results are presented, and a simple interpretation of the measured NICE-OHMS signal, as the sum of two dispersion signals, is given.

Contents

1 Introduction

1.1 Frequency Standards: Stability and Accuracy

What is a clock? Looking at an old fashioned pendulum clock, we see that it can be divided into two components: The pendulum and the clockwork. The pendulum supplies the clockwork with a frequency, and the clockwork uses this frequency to display the time, and supplies the pendulum with the energy needed to sustain oscillation.

All clocks schematically resembles the pendulum clock. E.g., in a modern electronic wrist watch the "local oscillator" (the pendulum) is just an electric oscillator regulated by a quartz crystal. A *frequency standard* is a device, capable of producing a stable and well known frequency. As such, the pendulum and the quartz crystal are examples of frequency standards [1]. Any stable frequency reference is a standard, if we can relate it to all other standards. This is to say that we need to know how many times it oscillates in a given period of time. The SI system uses the period called the second. Now one standard needs to be the defining standard, to which all other standards must be compared. Originally the second was defined as $1/(60 \cdot 60 \cdot 24)$ of a "mean solar day" [2]. That is, the rotation of the Earth was the defining standard. This is a good standard, because it is the same all over the world, unlike a pendulum or a piece of quartz, which also requires complete agreement on the definitions of length and weight, and may be affected by local parameters like pressure, humidity and variations in gravity.

The rotation of the Earth is, however, not a good standard, because it is not completely constant. So, in 1967 the 13^{th} General Conference on Weights and Measures redefined the second to be exactly "the duration of 9 192 631 770 periods of the radiation corresponding to the transition between the two hyperfine levels of the ground state of the caesium 133 atom" [1]. Quantum mechanics dictates that a certain kind of atom can be in certain discrete energy states, and when making transitions from one state to another it emits or absorbs a photon of frequency $\nu = E/h$, were E is the energy difference between the two levels, and h is Plancks constant. Since all atoms of the same kind are, to our best understanding, completely identical, this is an incredibly good standard.

This new definition, of course, was a reaction to the fact that atomic clocks had been developed, in which a local oscillator was being kept on resonance with an atomic transition, thereby constituting a highly stable clock.

A frequency standard is generally characterized by two parameters. Stability and accuracy. The *stability* is a measure of how well the oscillator reproduces the frequency it supplied at some earlier time, and the *accuracy* is a measure of how well we know the frequency of the oscillator. That is, in terms of the defining standard.

Atomic clocks using the defining standard, the microwave transition in a ^{133}Cs atom, are by definition the most accurate clocks. But atomic clocks using an optical transition in ^{87}Sr, is proving to be 1-2 orders of magnitude more stable than the best Cs clock at the moment. Being the more stable frequency standard, it is argued that it is time to redefine the second to this optical standard [3], [4].

An optical atomic clock is a clock that is referenced against an optical atomic transition, instead of a microwave transition, as in the conventional atomic clocks. A local oscillator for such a clock consists of a laser, stabilized against a ULE (Ultra Low Expansion) cavity, in an evacuated chamber. This kind of local oscillator is highly stable, especially on a short time

scale, but not necessarily accurate. Therefore it must be fine tuned to match the atomic reference. This is outlined in figure 1.1.

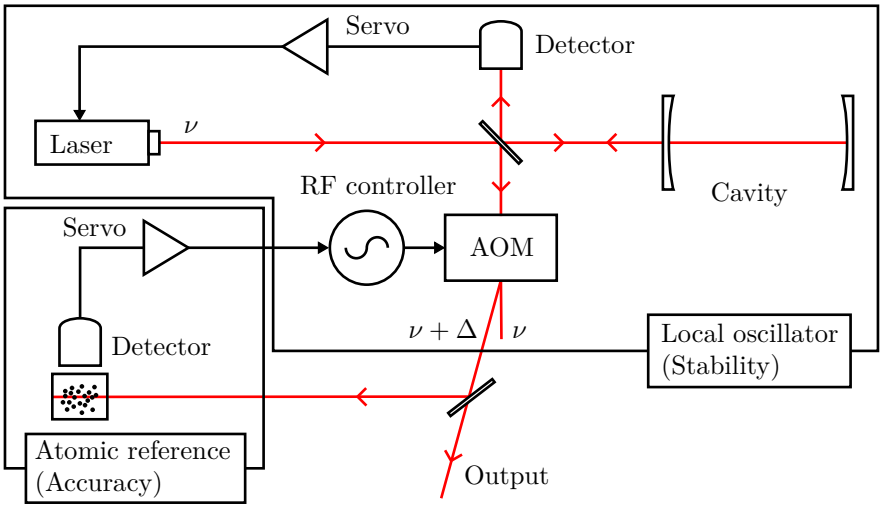

Figure 1.1: Schematics of a conventional optical clock. *Local oscillator:* A laser beam is incident on a cavity. If the frequency ν matches exactly the resonance of the cavity, no light is reflected from the cavity and detected. If the frequency is drifting, intensity is detected, and an error signal is generated and fed back to the laser, counteracting the drift. Part of the laser beam is directed into an acousto-optic modulator (AOM) driven by a radio frequency (RF) voltage, shifting the frequency by an amount Δ. The output from the local oscillator is $\nu + \Delta$. *Atomic reference:* Part of the local oscillator beam is shone on a sample of the reference atoms. If the frequency is on resonance, light will be absorbed and emitted in all directions (fluorescence). If the frequency is drifting, less fluorescence will be detected, and an error signal will be generated, and fed back to the local oscillator counteracting the drift.

1.2 Towards a New Optical Atomic Clock

We are proposing a new way to stabilize the laser frequency, instead of the conventional setup, using a ULE Cavity. There are theoretical predictions that a system consisting of a cavity with a trapped sample of ultracold atoms between the mirrors could provide a more sensitive error signal generation. That is, what we are aiming to achieve, is to improve the stability of the local oscillator. This is outlined in figure 1.2. It is important for this technique that the trapped atoms have a narrow transition in the optical frequency domain [5].

An error signal is a voltage signal, with a sign depending on whether the frequency is below or above resonance. The sensitivity, a measure of quality, depends on the steepness of the error signal at the point of zero-crossing.

As a first step towards building a more stable laser source, we need to examine the cavity-atom system, to learn more about what it does to the laser field. To do this we have constructed a local oscillator, stabilized against a ULE cavity, and use an acousto-optic modulator (AOM) to generate a spectrum of frequencies, that we can use to probe the cavity-atom system. This setup is shown in figure 1.3. For our atoms we use a sample of ^{88}Sr in our cavity.

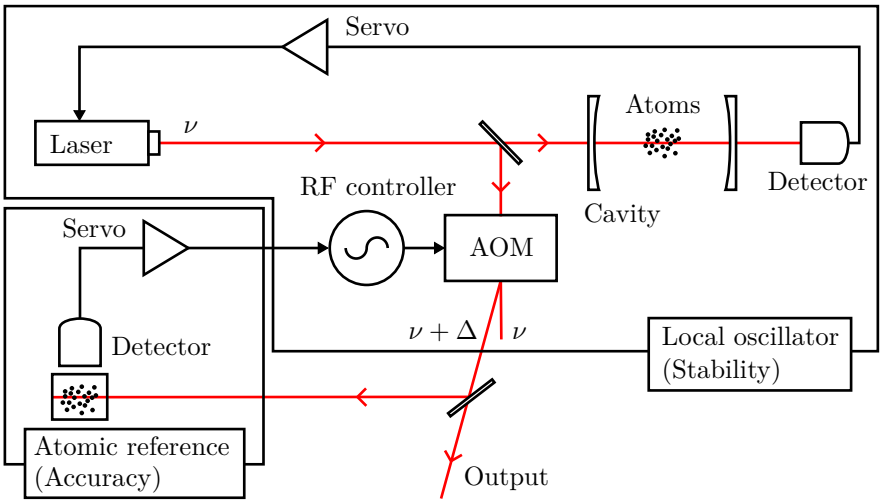

Figure 1.2: Ultracold atomic sample in cavity. A new method for frequency stabilization. This method should theoretically improve the stability of the local oscillator. The part of the setup with the atomic reference, maintaining accuracy, is the same as in figure 1.1.

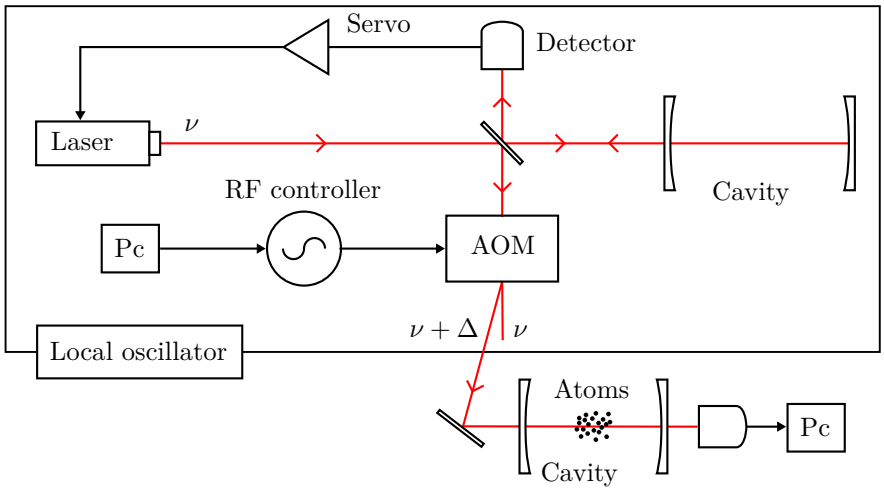

Figure 1.3: The experimental setup that we will be using to investigate the cavity-atom system. A regular ULE cavity stabilized local oscillator, shifted with an AOM, is used to generate a spectrum of stable, well known, frequencies for investigating the cavity-atom system.

In order to confine the atoms inside the cavity and keep their thermal motion in the mK range, we need to have an arrangement for producing ultracold atoms. Chapter 2 will be dedicated the description of this arrangement. In chapter 3 we will investigate the consequences of placing a sample of ultracold atoms in a cavity. What happens to the electric field transmitted through the cavity, and how do we use this to generate an error signal?

2 Ultracold ^{88}Sr Atoms

2.1 ^{88}Sr Energy Levels

We choose ^{88}Sr as our intracavity atoms, because of its advantageous energy level structure. Specifically it has:

- A broad, almost closed, transition, suitable for laser cooling and confinement of the atomic sample, at 460.73 nm (blue light).
- A narrow (non dipole allowed), closed, transition, suitable for performing the clock laser spectroscopy, at 689.3 nm (red light).

We will be concerned with the energy levels presented in figure 2.1. The transitions are numbered and their wavelengths, λ, and decay rates, A, are displayed in table 2.1. The two primary transitions of interest are coloured corresponding to their appearance.

	λ (nm)	A (s^{-1})	Ref.
1	460.73	2.01e8	[6]
2	6.5e3	3.9e3	[7]
3	1.8e3	6.6e2	[7]
4	1.9e3	1.34e3	[7]
5	679.1	8.9e6	[6]
6	687.8	2.7e7	[6]
7	707.0	4.2e7	[6]
8	689.3	4.69e4	[6]

Table 2.1: Vacuum wavelengths and decay rates for the relevant transitions in ^{88}Sr. Numbers refer to figure 2.1.

2.2 Overview of Experimental Setup

The technique used to cool and trap a small sample of ^{88}Sr atoms is laser cooling. Everything takes place in a vacuum chamber, to avoid disturbances from other atoms and molecules. A small amount of strontium is heated to about 550 °C in the *Oven* (basically just a hot metal cylinder with a small hole in one end). Part of the Sr-atoms evaporate and fill the volume of the oven. By diffusion a continuous beam of atoms escapes through the small hole, and enters the *Zeeman Slower*. The thermal velocities of the atoms approaches 500 m/s [8]. As the atoms travel through the Zeeman slower, they are decelerated to about 30 m/s. After this, the slow atoms enter the *Magneto Optical Trap (MOT)*, where they are confined in a small volume of about 0.5 cm^3, with velocities from 0.1 - 0.5 m/s. Slowing to a low velocity is necessary for the MOT to be able to capture the atoms [8].

Now the whole point of this is to trap the atoms between two *Cavity Mirrors*, so we simply place the mirrors outside two windows in the vacuum chamber. This is all shown in figure 2.2. In order to avoid AC Stark shifts and loss of coherence, we turn off the MOT light before probing the atoms with the clock frequency. Just after the MOT is turned off,

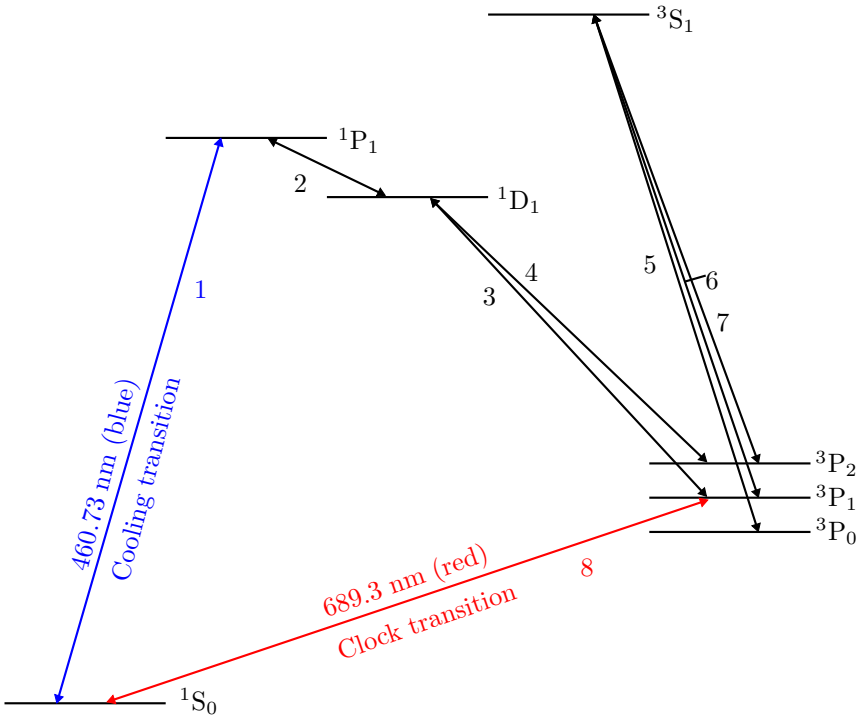

Figure 2.1: Relevant ^{88}Sr energy levels and transitions. Numbers refer to table 2.1.

the atoms are in free fall, and not affected by anything but the clock laser, just as we want it. After a couple of milliseconds the atoms have flown away and we need to load the MOT again to make a new measurement.

In the following sections the Zeeman slower and the MOT will be described.

2.3 Zeeman Slower

2.3.1 Basic Principle

The basic principle of laser cooling is to have fast atoms lose momentum, by absorbing photons moving in the opposite direction. When the photon is re-emitted in a random direction the atom of course gain the same momentum, but after absorbing and emitting a large number of photons, the random emission will average to zero, whereas the absorption always slows the atoms.

This simple basic principle, is slightly complicated by the fact that the atoms only will absorb photons approximately at resonance frequency, and the photon frequency experienced by the atoms depends on the atoms velocity, because of the Doppler effect. The obvious solution to this problem is to have the laser frequency increase quickly to match the resonance of the atoms all the way through the slower (this is called chirp cooling). A much simpler and more effective approach, devised by William Phillips (who was awarded the Nobel price in 1997, for this), uses the Zeeman effect to change the atomic energy levels. That is, a coil is wound around the tube, creating a spatially varying magnetic field, so that the atoms are kept in resonance with the Doppler shifted photon frequency [9].

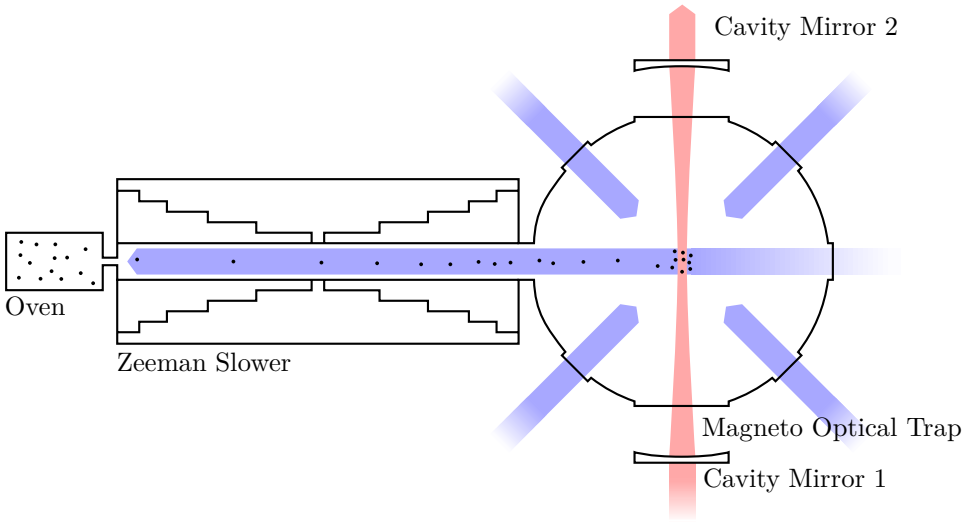

Figure 2.2: Overview of experimental setup for the cavity-atom technique. ^{88}Sr is evaporated in the oven; slowed from 500 m/s to 30 m/s in the Zeeman slower; and captured in the MOT between the two cavity mirrors. The setup is about 1 m in length.

2.3.2 Perturbation of the Detuning

The two energy levels involved in the cooling transition are $|^1\mathrm{S}_0\rangle$ and $|^1\mathrm{P}_1\rangle$ (see figure 2.1). When $|^1\mathrm{S}_0\rangle$ is subjected to an external magnetic field, B, nothing happens, as the total angular momentum of this state is 0. The state $|^1\mathrm{P}_1\rangle$, on the other hand splits up in three sublevels, whose energies depend on the orientation of the angular momentum, M_J, relative to the field. The energy difference between the ground state, $|^1\mathrm{S}_0\rangle$, and the Zeeman sublevels of $|^1\mathrm{P}_1\rangle$, is, to first order, given by [9]:

$$\begin{aligned} \Delta E &= E_0 + E_{ZE} \\ &= E_0 + g_J \mu_B B M_J. \end{aligned} \tag{2.1}$$

This is shown in figure 2.3. The Landé g-factor, g_J, is [9]:

$$\begin{aligned} g_J &= \frac{3}{2} + \frac{S(S+1) - L(L+1)}{2J(J+1)} \\ &= \frac{3}{2} + \frac{0 \cdot (0+1) - 1 \cdot (1+1)}{2 \cdot 1(1+1)} = 1. \end{aligned} \tag{2.2}$$

The (angular) resonance frequency is thus:

$$\begin{aligned} \omega_{res} &= (E_0 + E_{ZE})/\hbar \\ &= \omega_0 + \mu_B B M_J/\hbar. \end{aligned} \tag{2.3}$$

If the frequency of the cooling laser is ω_{laser}, and an atom is moving with velocity v_z towards the beam, the Doppler shifted frequency, experienced by the atom is [9]:

$$\omega_{doppler} = \omega_{laser} + k \cdot v_z. \tag{2.4}$$

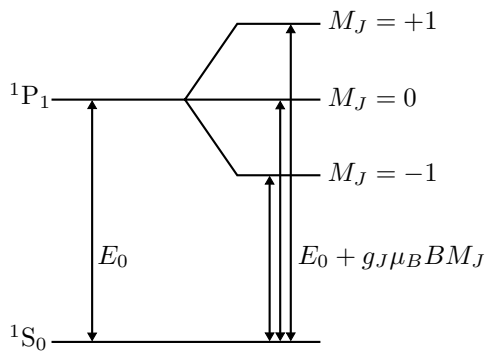

Figure 2.3: When a ^{88}Sr atom is subjected to a magnetic field B, the $|^1\mathrm{P}_1\rangle$-level is split into three Zeeman sublevels, and so is the transition energies.

The z-axis pointing from the oven towards the MOT. Using equation (2.3) and (2.4), the detuning experienced by the moving atom, in a magnetic field, B, is:

$$\begin{aligned} \delta &= \omega_{doppler} - \omega_{res} \\ &= \omega_{laser} + k \cdot v_z - \omega_0 - \mu_B B M_J/\hbar \\ &= \delta_0 + k \cdot v_z - \mu_B B M_J/\hbar. \end{aligned} \tag{2.5}$$

Where we define

$$\delta_0 \equiv \omega_{laser} - \omega_0, \tag{2.6}$$

as the detuning of the laser from the unperturbed stationary atom.

2.3.3 Computing Force and Required Magnetic Field

By Newtons second law, the decelerating force can be expressed as:

$$\begin{aligned} F &= (\text{photon momentum}) \times (\text{absorbtion rate}) \\ &= \hbar k \times (\text{emission rate}) \\ &= \hbar k \times A\rho_{22}. \end{aligned} \tag{2.7}$$

Where the fraction of the population in the excited state ρ_{22}, is determined by the optical Bloch equations. Expressing the steady state solution of ρ_{22} in terms of the field intensity, I, saturation intensity, I_{sat}, detuning, δ, and decay rate, A, we have [9]:

$$\begin{aligned} F &= \hbar k \frac{A}{2} \frac{I/I_{sat}}{1 + I/I_{sat} + 4\delta^2/A^2} \\ &= \hbar k \frac{A}{2} \frac{s_0}{1 + s_0 + 4\delta^2/A^2}. \end{aligned} \tag{2.8}$$

Here

$$s_0 \equiv I/I_{sat}, \tag{2.9}$$

is the so-called on-resonance saturation parameter. If we want the slower to be as short as possible, we should design the magnetic field, $B = B(z)$, such that the detuning, δ, is zero for the moving atoms, all the way trough the tube. Then the decelerating force, F, is at maximum all the time:

$$F_{max} = \hbar k \, \frac{A}{2} \, \frac{s_0}{1 + s_0}. \tag{2.10}$$

This, however, is not practical, because on resonance slowing is an unstable process. If an atom, e.g., accidentally emits a series of photons in the wrong direction, or just doesn't absorb photons for a little while, it doesn't slow down as it moves and therefore gets more and more out of resonance with the cooling laser, making the slowing force weaker and weaker. What we do, is decelerate the atoms with a laser frequency a little below resonance. I.e., with a force less than the maximum possible:

$$F = \epsilon \cdot F_{max} \ , \ \epsilon \sim 0.5. \tag{2.11}$$

In this way, if an atom misses a couple of photons, it will get more into resonance with the laser frequency, making photon absorption even more likely. This compensates for the missed photons until the atoms velocity again matches the intended trajectory.

Inserting equation (2.8) and (2.10) into (2.11), and solving for δ yields:

$$\delta = \pm \frac{A}{2} \sqrt{(1 + s_0) \frac{1 - \epsilon}{\epsilon}}. \tag{2.12}$$

Choosing the negative solution, so that an unintended high velocity will bring the detuning closer to resonance, and inserting equation (2.5), yields:

$$\begin{aligned} \delta_0 + k \cdot v_z - \mu_B B(z) M_J / \hbar &= -\frac{A}{2} \sqrt{(1 + s_0) \frac{1 - \epsilon}{\epsilon}} \\ B(z) &= \frac{\hbar}{\mu_B M_J} \left[\frac{A}{2} \sqrt{(1 + s_0) \frac{1 - \epsilon}{\epsilon}} + k v_z + \delta_0 \right]. \end{aligned} \tag{2.13}$$

A magnetic field with this z-dependence will slow the atoms effectively. But what is the z-dependence? One choice is to have s_0 constant, and therefore the deceleration constant. From a constant deceleration, $v_z(z)$ can be determined and inserted into equation (2.13). Thus the field is given, and the length of the slower determines the final velocity. However, as the atomic beam expands throughout the Zeeman slower, it makes sense to have the cooling laser beam follow this shape, as shown in figure 2.4. This ensures maximum overlap between laser beam and atomic beam, and additionally applies a small transverse force, counteracting the atomic beam expansion to some degree. When the beam is focused, the intensity, like v_z, becomes a function of z. And this must be taken into account when calculating the magnetic field. The on-axis intensity, I, of a Gaussian beam with absolute effect, P, and spot size, $w(z)$, is given by [10]:

$$I = \frac{2P}{\pi w(z)^2}. \tag{2.14}$$

Assuming constant expansion of the spot size from the entry, w_i, to the exit, w_o, the on-resonance saturation parameter is:

$$s_0(z) = \frac{2P}{\pi \left[w_i + \frac{z}{L}(w_o - w_i) \right]^2} \, \frac{1}{I_{sat}}. \tag{2.15}$$

Now the atoms are not subject to constant deceleration, which means that $v_z(z)$ must be determined by numerical integration.

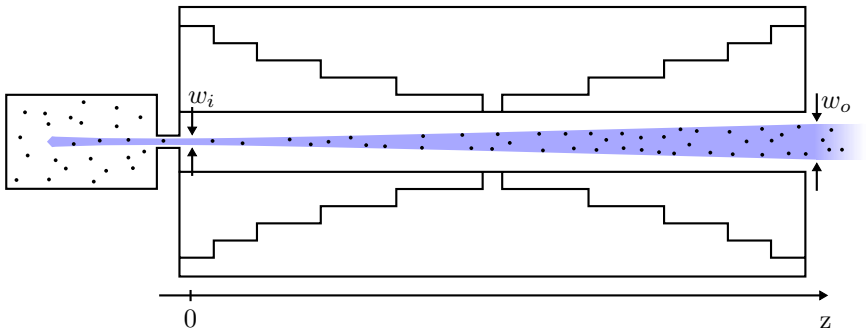

Figure 2.4: The atomic beam expands as it travels through the Zeeman slower. To follow this shape, the cooling laser beam is focused onto the oven aperture. w_i and w_o labels the spot size at the entrance and the exit of the Zeeman slower.

It is evident from equation (2.13) that the choice of Zeeman sublevel, M_J, determines the direction of the magnetic field, relative to the z-axis. We choose $M_J = -1$. Then the cooling beam must be σ^--polarized (left-handed relative to the z-axis), in order to have angular momentum conservation, during photon absorption. It is also seen that the choice of δ_0 gives an opportunity to change the offset of the field. We choose δ_0 such that the field is zero in the middle of the slower. This means that for the first half of the slower the field points towards the oven, and for the second half of the slower, the field points towards the MOT. In this way the absolute field strength is only half of what it would be, if we chose to have zero field at one of the ends. This makes it easier to realize practically [8].

For the cooling transition, $I_{sat} = \pi hcA/(3\lambda^3) = 42.8$ mW/cm^2 [9]. Choosing values for the parameters as in table 2.2, and having a maximum slowable velocity of 410 m/s, we numerically determine $v(z)$ using (2.11) and (2.15), and get an exit velocity of 23 m/s. Having determined $v(z)$ and $s_0(z)$ we get a magnetic field as presented in figure 2.5. The field has a minimum of -0.034 T and a maximum of 0.034 T.

In Appendix A the Matlab script used to determine $v_z(z)$ and $B(z)$, is presented.

ϵ	0.4	
P	32	mW
w_i	1	mm
w_o	8	mm
L	30	cm
δ_0	-3.5	GHz

Table 2.2: Parameters used to calculate the theoretical magnetic field shown in figure 2.5.

2.3.4 Simulating the Slowing Process

As described in [8] a coil is now wound around the tube, imitating, as well as possible, the theoretically calculated magnetic field. The slower coil is encapsulated in a magnetic shield, that both prevents the fields from the slower and the MOT to interfere with each other, and also enhances the slower field inside the tube. The measured magnetic field profile with and without shield, for a coil current of 21 A, is presented in figure 2.6. Instead of comparing the actual field with the theoretical field, we simulate what happens to atoms of different initial z-velocity, for different cooling beam powers P. The phase-space trajectories are presented

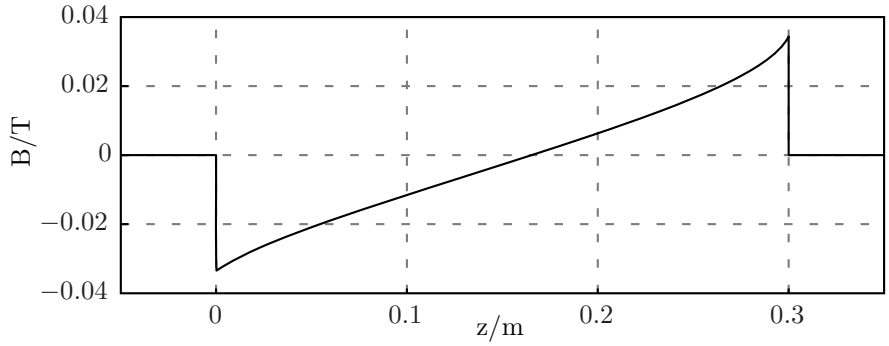

Figure 2.5: A magnetic field with this profile, and a cooling laser with parameters as in table 2.2, will slow an atom with initially maximum velocity 410 m/s to an exit velocity of 23 m/s.

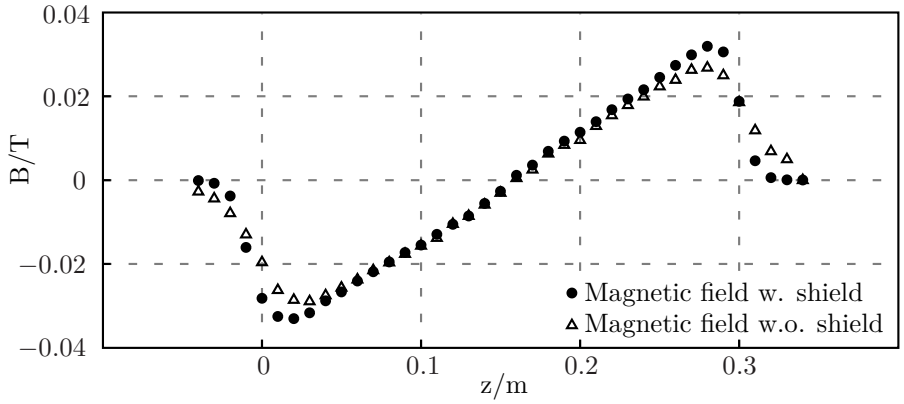

Figure 2.6: Measurements of the experimentally realized magnetic field, with and without magnetic shield, for a current of 21 A through the coil. It is seen that the shield help gaining a higher field peak magnitude, and helps terminating the field more abruptly at the slower entry and exit ($z = 0$ and $z = 0.3$) [measurements by Matin R.].

in figure 2.7. The Matlab script used for simulations can be found in Appendix B. We want the velocity for as many atoms as possible to be below the blue dashed line, indicating the estimated MOT capture velocity of 30 m/s [8]. It is seen that for low beam powers (∼10 mW), a lot of atoms is lost half way through the slower. For a power of about 14 mW, no atoms are lost half way any more. For higher powers (∼20 mW), atoms of higher initial velocities are slowed, but also more atoms are slowed below 0 m/s (i.e., they never make it out of the Zeeman slower). For beam powers of more than 22 mW, no atoms make it out of the slower.

2.4 Magneto Optical Trap

2.4.1 Basic Principle

We will not review any more than the very basic principles of the MOT. The physics needed to understand the MOT, is not any different from that needed for the Zeeman slower.

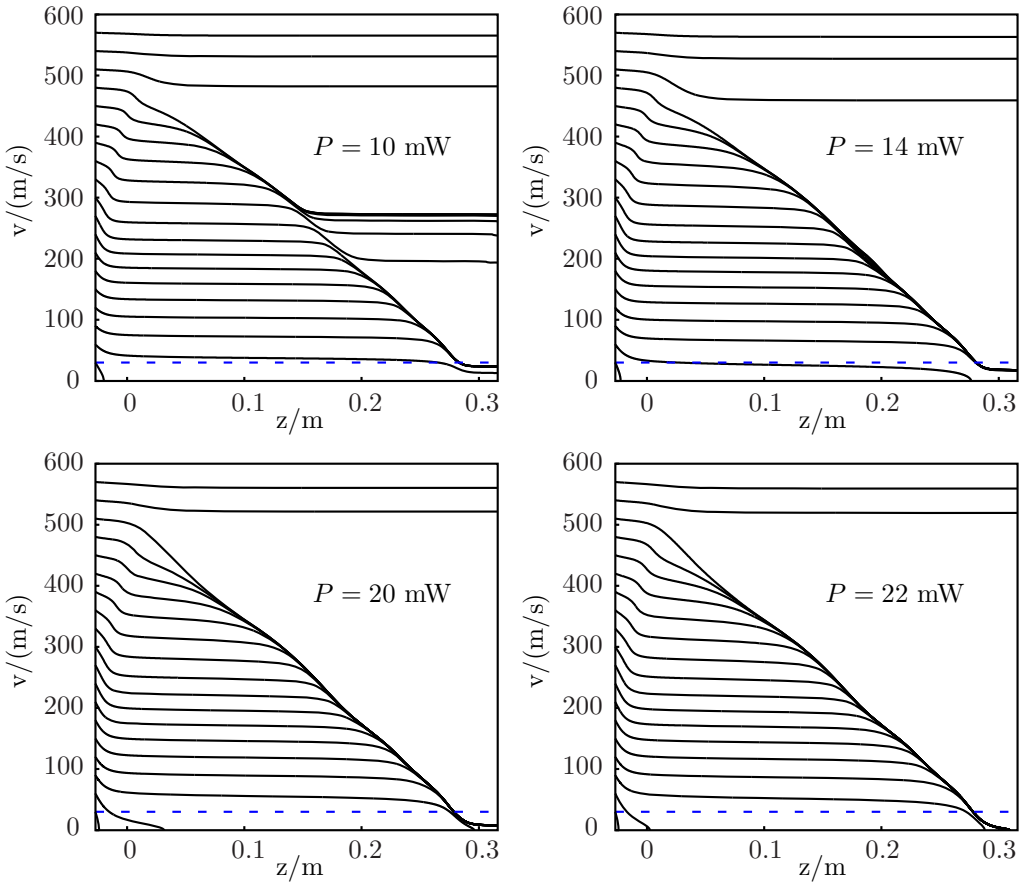

Figure 2.7: Simulated phase-space trajectories for different initial velocities, and four different cooling beam powers. The blue dashed line indicates the estimated MOT capture velocity of 30 m/s. For P = 10 mW, atoms are lost from the cooling process half way through the slower. For P = 14 mW, no atoms are lost during the slowing. For P = 20 mW, atoms of higher initial velocity are cooled, but also, some are brought to an actual stop (0 m/s), never leaving the slower. For P = 22 mW, all the slow atoms are brought to a complete stop before leaving the slower.

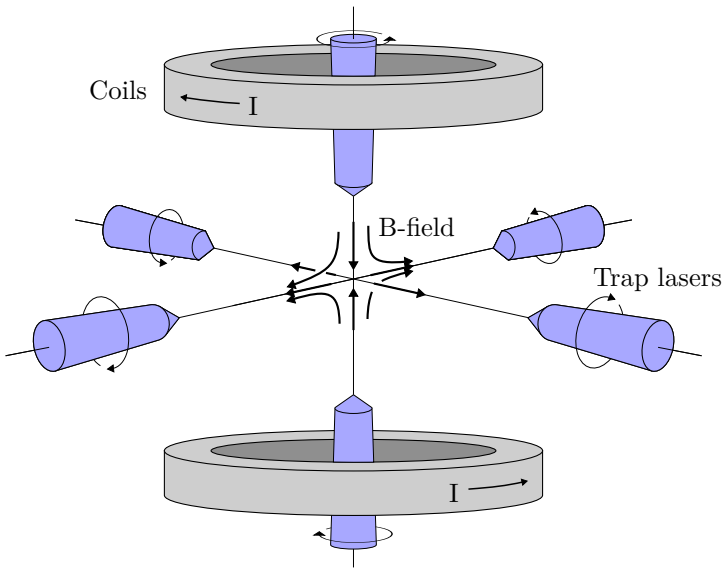

Figure 2.8: Schematics of the magneto optical trap. Two coils produce a magnetic field, that is zero exactly in the center. Six laser beams meets at this point. An atom displaced a little from the center is in resonance with the laser beam, because of the non zero B-field, and is pushed towards the center. The four lasers in the plane between the coils are the same as the ones depicted in figure 2.2. The beams are polarized to match the corresponding Zeeman sublevel.

Two electromagnetic coils are placed just over and under the vacuum chamber, creating a magnetic field, as shown in figure 2.8. The field exactly cancels in the middle of the chamber, and increases in all directions. It points away from the center in the plane of the four trap lasers (the four trap lasers also shown in figure 2.2), and points towards the center on the vertical axis, going through the coils. The six trap lasers are tuned a little below the resonance of the $|^1S_0\rangle \leftrightarrow |^1P_1\rangle$-transition. If an atom is displaced in some direction from the center, its energy levels are perturbed by the B-field, bringing it into resonance with the laser beam that pushes it towards the center. The beams are polarized to match the corresponding Zeeman sublevel [9].

Atoms approaching the center of the MOT with sufficiently low velocities will then get captured and trapped. Dispensed in mid-air they glow with the fluorescence of the blue trap light keeping them in place, easily seen through the top window of the vacuum chamber (see cover photo).

2.4.2 Repumpers

Investigating the energy level diagram in figure 2.1, it is evident that the cooling/trapping transition $|^1S_0\rangle \leftrightarrow |^1P_1\rangle$ is not quite a closed transition. When the atom is in the excited $|^1P_1\rangle$-state it will decay to the $|^1D_1\rangle$-state approximately 1 out of 50000 times ($A_2/A_1 \approx 1/50000$). From this it can decay to either $|^3P_1\rangle$ and from this back to the ground state, or, it can decay to the very long lived (dark) $|^3P_2\rangle$-state. Staying in this state, it is unaffected by the trap lasers, and it escapes the MOT. To prevent the atoms from staying there, we excite the atoms, with a 707.0 nm laser, to the $|^3S_1\rangle$-state, from which it can decay to the $|^3P_1\rangle$-state. For those that decay to the other dark state, $|^3P_0\rangle$, we have a 679.1 nm laser to excite them back. This way, by shining two (red) laser beams on the cold atomic cloud,

we avoid loosing the atoms by unwanted decay to dark states, and achieves as much as a factor of 10 more atoms in the MOT [7].

2.5 Testing the Zeeman Slower

The fluorescence of the trapped atoms is directly related to how many atoms the Zeeman slower decelerate below capture velocity. We want to measure how the atomic fluorescence depends on the power of the cooling beam, demonstrating, hopefully, the behaviour described by the simulations. A photomultiplier placed over the top window of the vacuum chamber measures the intensity of this fluorescence. The power of the laser beam is changed by adjusting the amplitude of the radio frequency signal fed to the AOM responsible for providing the detuning. The laser power is measured with a power meter.

It turns out that the Zeeman slower coil current, that provided the best MOT capture, was 7 A. The MOT coils are configured such that the magnetic field in the plane points away from the center (i.e., as in figure 2.8). In this way the field changes direction from the last part of the Zeeman slower to the MOT. We scan the whole range of beam powers available, and for each measurement, the repumpers are tuned to optimal MOT fluorescence, in case they are drifting in frequency. The plot of these measurements is presented in figure 2.9. We see, as we expect, that for low beam powers, we have very little fluorescence, and as

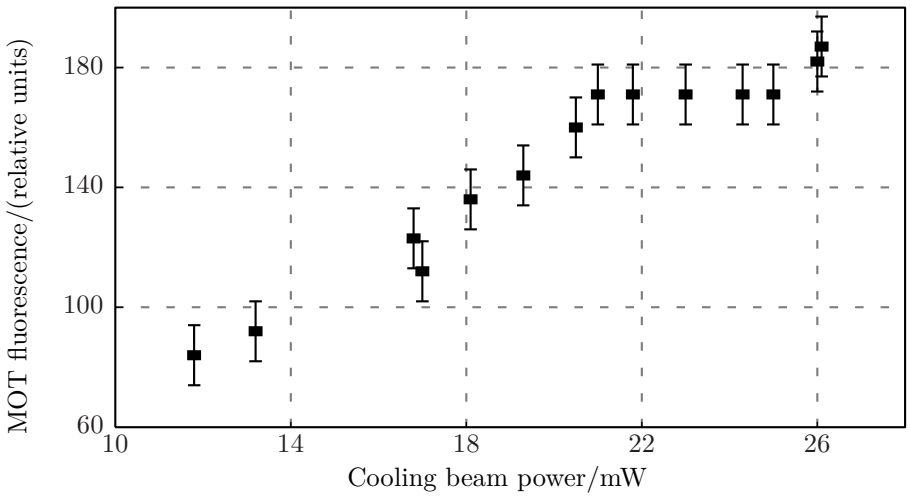

Figure 2.9: MOT fluorescence, measured with a photomultiplier, for different cooling beam powers. The Zeeman slower coil current is 7 A.

we crank up the power more and atoms are cooled and trapped. Around 22 mW no more atoms are trapped when the power is increased. This probably corresponds to atoms of higher initial velocity being slowed to under capture velocity, but also more of the initially slow atoms never making it out of the Zeeman slower. For even higher powers we would expect the fluorescence to start decreasing as fewer and fewer atoms make it out of the oven, unfortunately the laser power could not get any higher, making it impossible to demonstrate this behaviour.

That the optimal Zeeman slower current is 7 A, must mean that we are nowhere near slowing and trapping all the velocity classes from 100 - 500 m/s as in the simulations. A current of 7 A results in only one third of the field, measured at 21 A. A more detailed simulation taking into account the off axis laser beam intensity and transverse heating of the atomic beam, could perhaps explain this.

Another way of configuring the setup, is to invert the current in the MOT coils. This way the field in the last part of the Zeeman slower and the region from the Zeeman slower to the center of the MOT points in the same direction. This effectively extends the Zeeman slower all the way to the center of the MOT. It turns out that for this configuration a Zeeman slower coil current of 10 A is optimal. The result of the measurements for this configuration is displayed in figure 2.10. It is seen that this is a more effective way of operating the setup, as the MOT intensity is almost twice as high. The same, expected, dependenc the beam power is observed here. This time, it is not completely evident if we reach the optimal beam power, or if we would actually benefit a little from being able to turn up the power 2-3 mW.

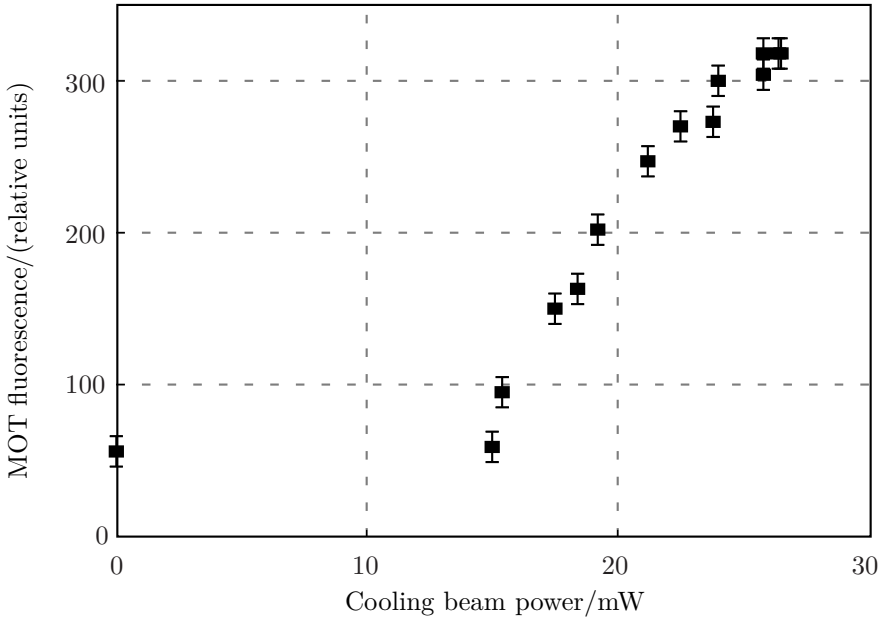

Figure 2.10: MOT fluorescence, measured with a photomultiplier, for different cooling beam powers. The Zeeman slower coil current is 10 A. This time the magnetic field of the MOT is inverted, such that the MOT field in the plane points in the same direction as the Zeeman slower field, in the last half of the slower. This way the Zeeman slower is practically extended all the way to the center of the MOT.

In conclusion, calculations and simulations, gives an order-of-magnitude idea about how to realize the desired arrangement with ultracold atoms. Then, by experimentally tweaking the available degrees of freedom in the setup, we achieve the goal of loading a MOT properly with a great number of atoms. Thus we are ready to move on.

3 Producing the Error Signal

3.1 The Basic Idea

An electric field transmitted through a Fabry-Perot cavity with ultracold atoms will undergo a phase shift due to the atoms and due to the cavity. The profile of the phase shift due to the atoms has a steep slope around the atomic resonance. This we will use as an error signal, for stabilizing the frequency of a laser, constituting the local oscillator of an optical atomic clock. In order to measure the phase shift we make use of the so-called NICE-OHMS technique, and for this technique to work, it is necessary to lock the cavity to the probe laser frequency, such that the transmission is maximum all the time. Thus we start by going through the cavity-atom system, and describe the acquired phase shift. Afterwards the Hänsch-Couillaud cavity locking method and finally the NICE-OHMS technique is explained.

3.2 Fabry-Perot Cavity with Ultracold Atoms

To examine what happens to an electric field transmitted through a Fabry-Perot cavity with a sample of atoms in the middle, we start by reviewing the Fabry-Perot cavity without atoms. For at field of amplitude E_{in}, normally incident on a cavity with mirrors of transmission, t, and reflectivity, r, we get a transmitted wave of amplitude [10]:

$$\begin{aligned} E_t &= E_{in}t^2e^{ikL} + E_{in}t^2r^2e^{ik3L} + E_{in}t^2r^4e^{ik5L} + ... \\ &= E_{in}t^2e^{ikL}\left[1 + r^2e^{ik2L} + r^4e^{ik4L} + ...\right] \\ &= E_{in}t^2e^{ikL}\left[\frac{1}{1-r^2e^{ik2L}}\right]. \end{aligned} \tag{3.1}$$

As is seen in figure 3.1.

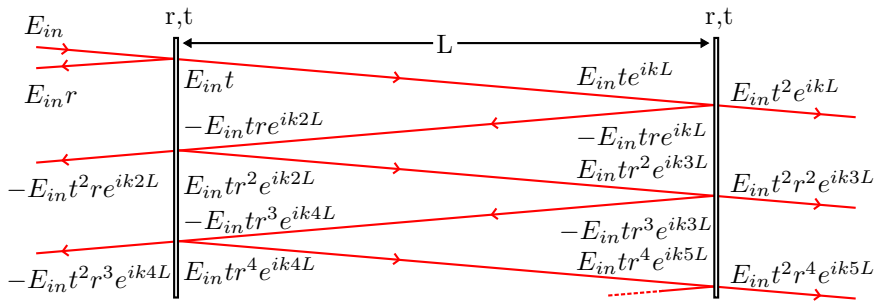

Figure 3.1: Reflection and transmission from a Fabry-Perot cavity. The beam has been tilted so that the intracavity development of the complex amplitude can be traced. The transmitted total amplitude, from a field, normally incident on the cavity, is the sum of all the partial transmissions.

Now we introduce the intracavity atomic sample. By putting the sample on the path between the two mirrors as in figure 3.2, it introduces a complex phase shift, β, to the field

each time it passes. Now the transmitted field is instead:

$$E_t = E_{in}\frac{t^2 e^{i(kL+\beta)}}{1 - r^2 e^{i(k2L+2\beta)}}. \tag{3.2}$$

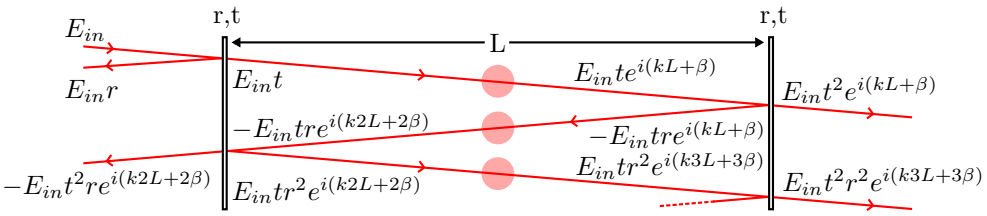

Figure 3.2: Fabry-Perot cavity, with an atomic sample. The sample changes the amplitude of the field by a complex factor of $e^{i\beta}$, each time it passes.

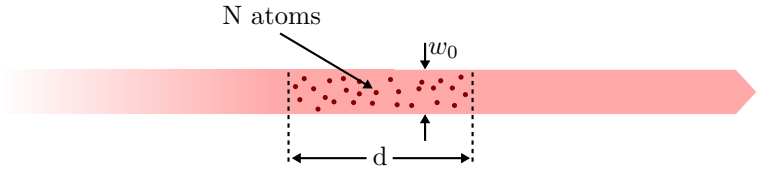

Figure 3.3: The probe beam, with waist w_0, traverses a distance, d, through the atomic cloud, overlapping N atoms.

We simply treat the atomic cloud as a medium of refractive index n. As illustrated in figure 3.3, the field passes a distance, d, through the medium, gaining a complex phase shift, knd, instead of kd as it would if no medium were present. Thus the acquired complex phase shift due to the atoms is:

$$\begin{aligned}\beta &= knd - kd \\ &= k(n-1)d.\end{aligned} \tag{3.3}$$

From classical electromagnetic theory [10] the refractive index, n, is given by:

$$\begin{aligned}n &= \sqrt{1 + \frac{\alpha}{\epsilon_0}N/V} \\ &\approx 1 + \frac{\alpha}{2\epsilon_0}N/V \quad , \quad \text{assuming } n \approx 1.\end{aligned} \tag{3.4}$$

Where α is the polarizability of a single atom, and N/V is the number of atoms per volume. With a beam area of $A = \pi w_0^2/4$, we get a phase shift:

$$\begin{aligned}\beta &= k\left[\frac{\alpha}{2\epsilon_0}N/V\right]d \\ &= \frac{k\alpha N}{2\epsilon_0 A} \\ &= \frac{2kN}{\epsilon_0 \pi w_0^2}\,\alpha.\end{aligned} \tag{3.5}$$

Where N is simply the absolute number of atoms covered by the beam. A more rigorous, and less simplified analysis is given in [11]. Now, the complexity of β originates from the

polarizability, $\alpha = \alpha_R + i\,\alpha_I$, of the atoms. The polarizability is defined as:

$$\boldsymbol{p} = \mathrm{Re}\{\alpha \boldsymbol{E}\}. \tag{3.6}$$

From quantum mechanics we know that [9]:

$$\boldsymbol{p} = -e\boldsymbol{X}_{12}\left[U\cos(\omega t) - V\sin(\omega t)\right]. \tag{3.7}$$

Setting equation (3.6) and (3.7) equal to each other, we get:

$$\begin{aligned}
\mathrm{Re}\{(\alpha_R + i\alpha_I)\boldsymbol{E}_0[\cos(\omega t) - i\sin(\omega t)]\} &= -e\boldsymbol{X}_{12}\left[U\cos(\omega t) - V\sin(\omega t)\right] \\
\left[\alpha_R\cos(\omega t) + \alpha_I\sin(\omega t)\right]\boldsymbol{E}_0 &= -e\boldsymbol{X}_{12}\left[U\cos(\omega t) - V\sin(\omega t)\right] \\
\alpha_R\cos(\omega t) + \alpha_I\sin(\omega t) &= \frac{e|X_{12}|^2}{\boldsymbol{E}_0\cdot\boldsymbol{X}_{12}}\left[-U\cos(\omega t) + V\sin(\omega t)\right] \\
\alpha_R\cos(\omega t) + \alpha_I\sin(\omega t) &= \frac{e^2|X_{12}|^2}{\Omega\hbar}\left[-U\cos(\omega t) + V\sin(\omega t)\right].
\end{aligned} \tag{3.8}$$

For this to hold in general, the coefficients of the sine and cosine terms must be equal, yielding:

$$\begin{aligned}
\alpha_R &= -\frac{e^2|X_{12}|^2}{\Omega\hbar}\,U, \\
\alpha_I &= \frac{e^2|X_{12}|^2}{\Omega\hbar}\,V.
\end{aligned} \tag{3.9}$$

This tells us that the real and imaginary part of $\beta = \beta_R + i\,\beta_I$ is directly proportional to U and V, respectively. From

$$e^{i\beta} = e^{i\beta_R}e^{-\beta_I}, \tag{3.10}$$

it is evident that $\beta_R \propto \alpha_R \propto -U$ determines the actual phase shift, whereas $\beta_I \propto \alpha_I \propto V$ is responsible for an attenuation (i.e., absorption).

Solving the optical Bloch equations for the steady state solution ($t \to \infty$) yields [9]:

$$\begin{aligned}
U(\omega) &= \frac{\Omega(\omega - \omega_0)}{(\omega - \omega_0)^2 + \Omega^2/2 + A^2/4}, \\
V(\omega) &= \frac{\Omega A/2}{(\omega - \omega_0)^2 + \Omega^2/2 + A^2/4}.
\end{aligned} \tag{3.11}$$

The frequency dependencies of U and V are depicted in figure 3.4. Notice the above mentioned steep slope of the phase shift, $\beta_R \propto -U$, around resonance. But these are steady state solutions, and we have a sample of ultracold atoms suddenly released from being driven on the very broad cooling transition. So we must expect a very coherent response from the atoms, that all suddenly drops to the ground level, and starts responding to the probe beam. Numerically integrating the optical Bloch equations shows that steady state occurs around 100 μs. See figure 3.5. The Matlab Runge Kutta script is shown in Appendix C.

3.3 Hänsch-Couillaud Cavity Locking Method

In order to have maximum transmission, we need to ensure that the length of the cavity, containing the atoms, stays in resonance with the probe frequency. In order to do this, we make use of a special technique developed by T. W. Hänsch and B. Couillaud in 1980. Originally, they developed this technique, to lock a laser frequency to a cavity [12]. We use it, reversely, to lock the cavity length to the laser frequency. As shown in figure 3.6, a linear polarizer is placed inside the cavity, and the field reflected from the cavity is analysed, by

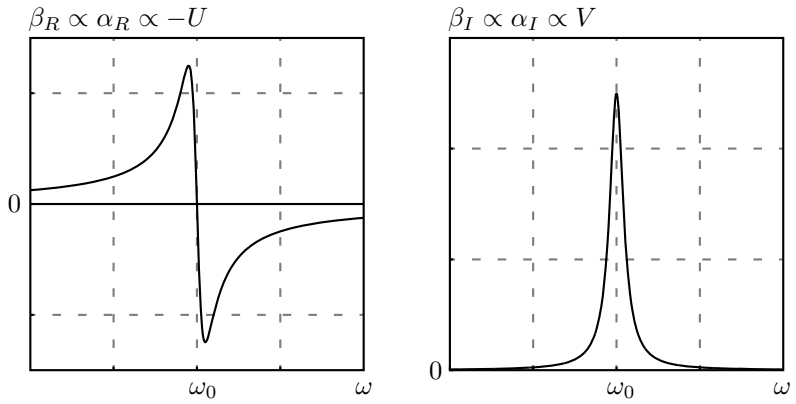

Figure 3.4: Dispersion ($\beta_R \propto \alpha_R \propto -U$), and absorption ($\beta_I \propto \alpha_I \propto V$), as functions of probe frequency, for the steady state solution of the optical Bloch equations (arbitrary units).

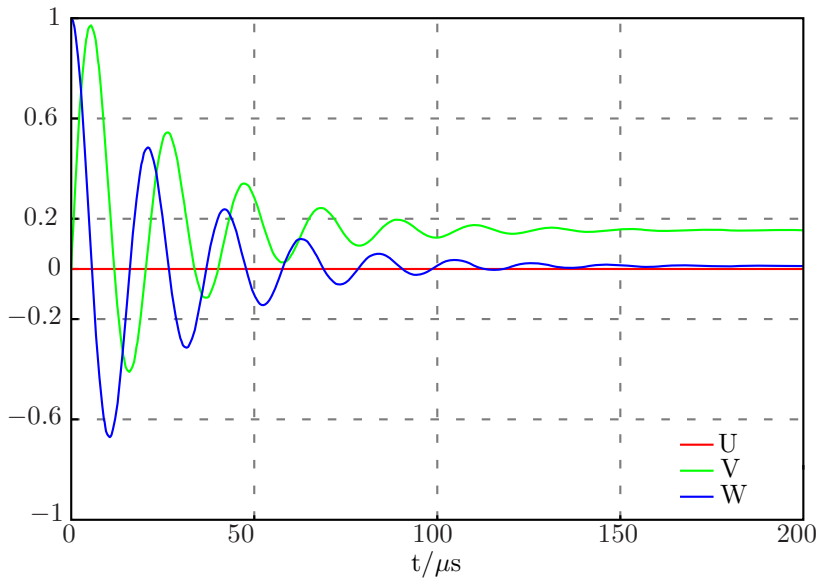

Figure 3.5: Time dependencies of U, V, and W. Numerically integrated, for a decay rate A = 4.69e4 s^{-1}, zero detuning, a Rabi frequency of 300kHz, and all the atoms initially in the ground state. The relaxation time is maximum for zero detuning and independent of the Rabi frequency. It is seen that steady state occurs approximately around 100 μs.

directing it through a $\lambda/4$-waveplate, dividing it with a polarizing beam splitter (PBS), and comparing the two different intensities. This works as follows: Linearly polarized light is incident on the cavity. This can be considered as a superposition of a component parallel to the direction allowed by the linear polarizer ($E_{in\parallel}$), and a component perpendicular to this direction ($E_{in\perp}$). The perpendicular field reflected by the cavity is simply

$$E_{r\perp} = rE_{in\perp}, \tag{3.12}$$

since the part of the field transmitted into the cavity is completely extinguished by the polarizer. The parallel part of the reflected field is, on the contrary, also determined by the contributions from the field inside the cavity. From figure 3.2 we get:

$$\begin{aligned} E_{r\parallel} &= rE_{in\parallel}\left[1 - t^2 e^{i(k2L+2\beta)}\left[1 + r^2 e^{i(k2L+2\beta)} + r^4 e^{i(k4L+4\beta)} + ...\right]\right] \\ &= rE_{in\parallel}\left[1 - \frac{t^2 e^{i(k2L+2\beta)}}{1 - r^2 e^{i(k2L+2\beta)}}\right]. \end{aligned} \tag{3.13}$$

That is, $E_{r\perp}$ is always the same, whereas $E_{r\parallel}$ is dependent on the properties of the cavity and the atoms. If the laser frequency is on resonance with the cavity-atom system ($k2L + 2\beta_R = m \cdot 2\pi$), then the factor in the parenthesis multiplying $E_{in\parallel}$ is real, and the total reflected wave is a linearly polarized field. If, however, the laser frequency is not on resonance with the system, $E_{r\parallel}$ will suffer a positive or negative phase shift, depending on whether the frequency is below or above resonance. The total reflected field will be elliptically polarized, with handedness determined, again, by whether the frequency of the laser is below or above the resonance of the cavity-atom system.

This means that we want to determine whether the total reflected, generally elliptic, field is left-handed or right-handed polarized. Now an elliptically polarized field can be thought of as a superposition of a left- and a right-handed circularly polarized fields, with different amplitudes. The one with the greater amplitude determining the handedness of the total field. Linearly polarized light corresponds to exactly equal amplitudes. The $\lambda/4$-plate changes these two circularly polarized fields into two linearly polarized beams orthogonal to each other ($\pm 45°$ to the optical axis of the waveplate). Aligning the waveplate such that the optical axis is at exactly 45° to the PBS, we can split the two linear components, and measure them with two detectors. If the two detectors receive equal amount of power, then the frequency is on resonance, but if one receives more than the other, then it tells us that $E_{r\parallel}$ is phase shifted to one side. A differential amplifier generates an error signal by subtracting one power from the other. This error signal is then fed to a piezoelectric crystal that changes the length of the cavity in the direction necessary to bring it into resonance with the laser frequency.

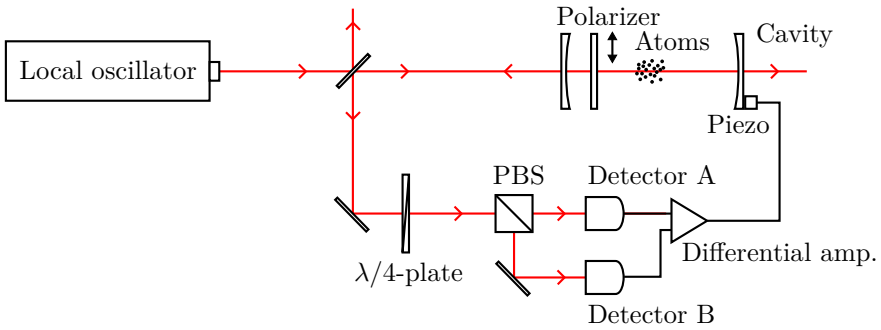

Figure 3.6: Diagram of the optical setup for a Hänsch-Couillaud cavity lock. The local oscillator is the one described in figure 1.3. The handedness of the reflected field tells whether the local oscillator frequency is below or above resonance of the cavity. This is used to continuously adjust the length of the cavity, with a piezoelectric crystal, keeping it in resonance with the local oscillator frequency.

It is crucial for all this to work, that the incoming field is not completely parallel to the direction allowed by the linear polarizer. On the other hand, the angle must not be too

large either, since this will mean less transmitted intensity. We choose the angle such that $E_{in\perp} \sim 5\%$ of E_{in}.

3.4 NICE-OHMS Technique

This technique, that is an acronym for *"Noise-Immune Cavity-Enhanced Optical Heterodyne Molecular Spectroscopy"* [13], offers a way of measuring the phase shift, imposed by the atoms, of the output field from the cavity. The probe (carrier) frequency, ω, is modulated by an electro-optic modulator (EOM) to have two sidebands with frequencies $\omega - \Omega$ and $\omega + \Omega$. Ω is chosen to be exactly equal to the free spectral range (FSR) of the cavity. This is all illustrated in figure 3.7. The modulated field, sent into the cavity, is given by:

$$E_{in} = J_0 e^{i\omega t} + J_1 e^{i(\omega+\Omega)t} - J_1 e^{i(\omega-\Omega)t}. \tag{3.14}$$

Here J_0 and J_1 are Bessel functions of the first kind, determined by the amplitude of the EOM driving frequency, Ω. For our purpose they are simply constants.

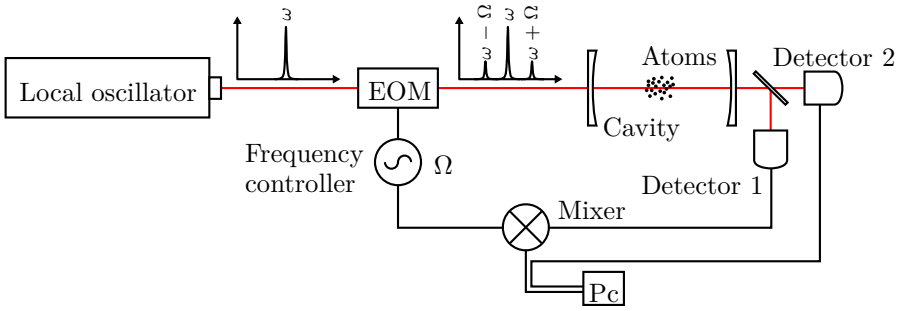

Figure 3.7: Schematics of the setup for performing NICE-OHM spectroscopy. An electro-optic modulator (EOM) supplies the carrier frequency, from the local oscillator (from figure 1.3), with two sidebands displaced exactly one free spectral range (FSR) from the carrier. Because the carrier frequency is affected by the atoms in the cavity, and the sidebands are not, the carrier will be phase shifted relative to the sidebands. A signal proportional to this phase shift is created by the use of Detector 1 and a mixer. Detector 2 measures the transmitted intensity, i.e., the atomic absorption.

Because the carrier frequency is locked to the resonance of the cavity-atom system, the two sidebands does, generally, not completely coincide with the resonances of the cavity, as illustrated in figure 3.8. The resonance of the cavity is:

$$\begin{aligned} k_{res}2L + 2\beta_R &= m \cdot 2\pi \\ \omega_{res}2L/c &= m \cdot 2\pi - 2\beta_R \\ \omega_{res} &= m\frac{\pi c}{L} - \frac{\beta_R c}{L} \\ \omega_{res} &= m\frac{\pi c}{L} - \Delta. \end{aligned} \tag{3.15}$$

Where

$$\Delta \equiv \frac{\beta_R c}{L}, \tag{3.16}$$

is vanishing for frequencies far from from the atomic resonance but significant close to. By choosing $\Omega = \text{FSR}$ we get an expression for the sideband frequencies in terms of the shift in the carrier resonance, Δ, due to the atoms (c.f., figure 3.8):

$$\omega \pm \Omega = (m \pm 1)\frac{\pi c}{L} - \Delta \tag{3.17}$$

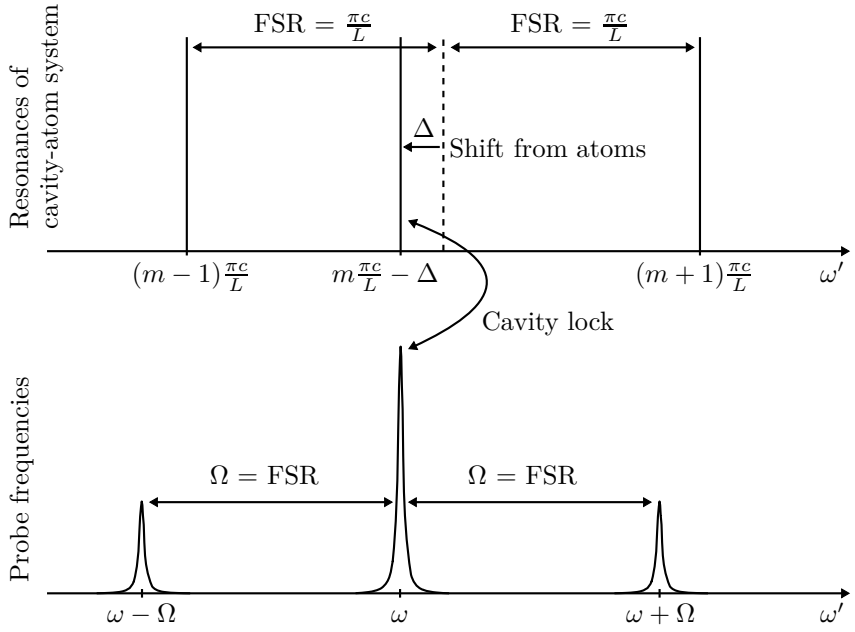

Figure 3.8: The cavity resonance $m\frac{\pi c}{L} - \Delta$ is locked to the carrier frequency ω. This means that the sideband frequencies are shifted exactly Δ below the cavity resonances.

Looking at the transmitted amplitude of the sidebands, with wavenumber $k_\pm$, using (3.2) and (3.17), assuming $\beta = 0$ (sideband frequencies far from atomic resonance), we get:

$$\begin{aligned} E_t/E_{in} &= \frac{t^2 e^{ik_\pm L}}{1 - r^2 e^{i2k_\pm L}} \\ &= \frac{t^2 e^{i(\omega \pm \Omega)L/c}}{1 - r^2 e^{i2(\omega \pm \Omega)L/c}} \\ &= \frac{t^2 e^{i((m\pm 1)\frac{\pi c}{L} - \Delta)L/c}}{1 - r^2 e^{i2((m\pm 1)\frac{\pi c}{L} - \Delta)L/c}} \\ &= e^{i(m\pm 1)\pi} \frac{t^2 e^{-i\Delta L/c}}{1 - r^2 e^{-i2\Delta L/c}}. \end{aligned} \tag{3.18}$$

Notice that, for any integer value of m, this quantity, the complex amplitude, is the same for both $+$ and $-$, i.e., the complex phase shift is the same for both sidebands. For small Δ, this complex amplitude is, expressed in terms of the carrier frequency phase shift:

$$\begin{aligned} E_t/E_{in} &= \pm \frac{t^2 e^{-i\beta_R}}{1 - r^2 e^{-i2\beta_R}} \\ &\approx \pm e^{-i(1+2\frac{r^2}{t^2})\beta_R}. \end{aligned} \tag{3.19}$$

I.e., the sidebands are phaseshifted an amount,

$$\phi \approx -(1 + 2\frac{r^2}{t^2})\beta_R, \tag{3.20}$$

relative to the carrier frequency. Because the cavity is locked to the carrier frequency, this component will experience no phase shift. But as phase shifts are completely relative, we might as well say that the carrier experiences a phase shift, ϕ, and the phase of the sidebands are unchanged by the cavity-atom system. Neglecting all attenuation, we then have:

$$\begin{aligned} E_{out} &= J_0 e^{i(\omega t+\phi)} + J_1 e^{i(\omega t+\Omega t)} - J_1 e^{i(\omega t-\Omega t)} \\ &= e^{i\omega t}\left[J_0 e^{i\phi} + J_1\left(e^{i\Omega t} - e^{-i\Omega t}\right)\right] \\ &= e^{i\omega t}\left[J_0 e^{i\phi} + i2J_1 \sin(\Omega t)\right]. \end{aligned} \tag{3.21}$$

We measure the intensity of the transmitted field, as shown in figure 3.7. This is proportional to:

$$\begin{aligned} |E_{out}|^2 &= E_{out} \times E_{out}^* \\ &= e^{i\omega t}\left[J_0 e^{i\phi} + i2J_1 \sin(\Omega t)\right] \times e^{-i\omega t}\left[J_0 e^{-i\phi} - i2J_1 \sin(\omega t)\right] \\ &= J_0^2 + i2J_0 J_1 \sin(\Omega t)[e^{-i\phi} - e^{i\phi}] + 4J_1^2 \sin^2(\Omega t) \\ &= J_0^2 + 2J_1^2 - 2J_1^2 \cos(2\Omega t) + 4J_0 J_1 \sin(\Omega t)\sin(\phi). \end{aligned} \tag{3.22}$$

That is, the intensity of the transmitted field is oscillating at two frequencies: 2Ω and Ω. We direct the measured signal into a mixer, also connected to the EOM frequency controller. Here the amplitude of the component oscillating at frequency Ω is picked out, and collected as data. This amplitude is proportional to $\sin(\phi)$, which is, assuming a small phase shift, approximately equal to ϕ, which is, by (3.20), proportional to $-\beta_R$. This is the NICE-OHMS signal. It is "*Noise-Immune*" because only the high frequency component, $\Omega/(2\pi) =$ 500 MHz, is relevant, whereas background noise, like regular audible sound waves, primarily resides in a frequency domain much lower than this. As seen in figure 3.7, there is also a detector that simply measures the intensity without the use of a mixer. This signal indicates the absorption from the atoms, however, with a much lower signal-to-noise ratio.

The NICE-OHMS signal is what we are proposing to use as an error signal for stabilization of a laser. It is shown how it is directly proportional to the phase shift introduced by the atoms.

3.5 Doppler Shift and Saturation

Even though we have cooled the atoms to very low velocities, they are not completely stationary. We roughly divide the atoms into three groups: one is moving towards the entrance mirror, one is almost stationary, and one is moving towards the output mirror. Velocity components perpendicular to the cavity axis are irrelevant to this matter. Now a beam with frequency higher than the atomic resonance will be in resonance with the group moving away from the direction of propagation, because of the Doppler effect. That is, the beam interacts primarily with one group, when it propagates one way, and the opposite group on its way back. The same goes for frequencies below the atomic resonance. For frequencies approximately at resonance, however, the beam interacts with the stationary group, both ways. This is shown in figure 3.9.

We expect this one-dimensional velocity distribution to be approximately symmetrical around zero. With maximum at zero. However for high probe intensities, the stationary group of atoms will be saturated to a higher degree than the atoms with velocity components towards one of the mirrors. Thus, one could argue that we get an effective velocity

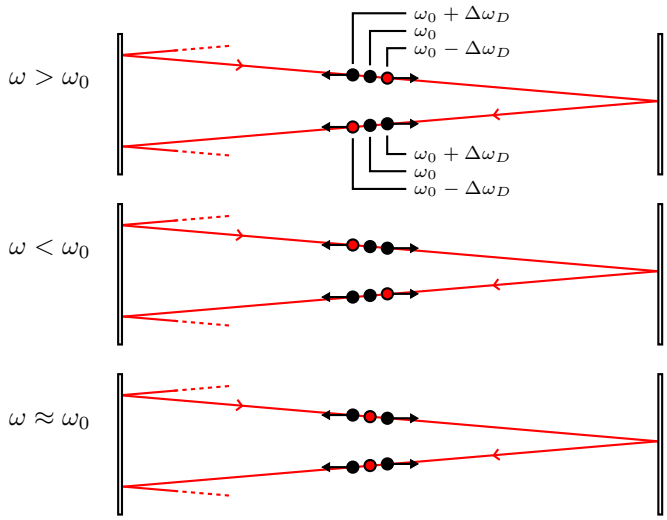

Figure 3.9: Dividing the atoms into three velocity groups. For positive (negative) detunings the beam will interact the strongest with atoms moving away from (towards) the beam. As the beam is reflected back and forth through the cavity, the beam interacts strongly with two different velocity groups. For small or no detuning, the beam only interacts the strongest with the stationary velocity group. The group that is most strongly interacting is coloured red.

distribution with two maxima at each side of zero. This yields two Doppler shifted resonances, i.e., two dispersion signals. Arguing this way, we expect the NICE-OHMS signal to look like the sum of two dispersion signal, as in figure 3.10.

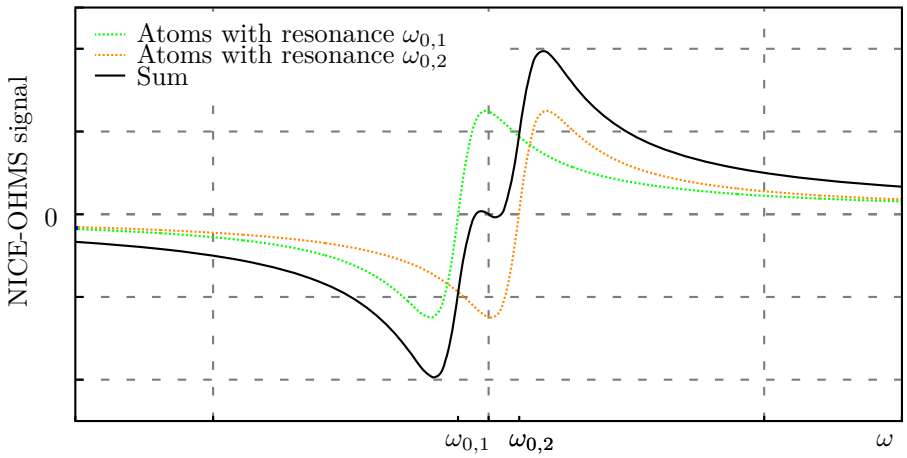

Figure 3.10: Hypethetical NICE-OHMS signal for an atomic sample with two resonances close to each other. Calculated as the sum of the NICE-OHMS signals for two atomic samples with two resonances. The NICE-OHMS signal has been assumed proportional to $-\beta_R$.

3.6 Collective Effects

The motivation for using this system as a stabilizing mechanism, is that we expect the slope of the NICE-OHMS signal, to be steeper than the error signal produced by a conventional ULE cavity. It is crucial for this to happen, that we observe a certain collective behaviour from the intracavity atoms around resonance. The idea is that because the atoms are subjected to a standing wave, as opposed to a travelling wave, the atoms will be driven completely in phase, between adjacent nodes. In the case of a travelling wave, the atoms are all driven with a small difference in phase due to the spatial dependency of the wave. All oscillating completely in phase, the atoms influence the field in a slightly different way than otherwise, which contributes to increasing the slope of the NICE-OHMS signal, used as an error signal. This is not obvious from the argument presented in the previous section. But this is also a highly simplified model. Given more time it would definitely pay off to go into a more detailed analysis of the cavity-atom system, treating each atom as an individual oscillator, responding to a standing wave, emitting radiation in all directions. And taking different velocity distributions into account.

3.7 Display of Data

The experimental arrangement includes a computer interface from which the range of frequencies and the resolution is controlled. A dataset is produced by loading the MOT; quickly turning of the trap light; and after a while (optimally, 100μs, according to the argument presented in section 3.2) the NICE-OHMS value, and the transmission value for the given probe frequency is collected as an average of the detected value over some time ($\sim 100\mu$s). This is repeated a number of times for different probe frequencies. Thus obtaining NICE-OHMS signal, and transmission signal as functions of probe frequency. A broad scan around the atomic resonance, is presented in figure 3.11 (transmission), and 3.12 (NICE-OHMS). We expect to see some sign of saturation around the center of the transmission profile. We do not. But also this detector was expected to be very sensitive to noise, as opposed to the NICE-OHMS signal. Looking at the NICE-OHMS signal it certainly looks a lot like the signal in figure 3.10. Except, the small wrinkle in the middle, due to saturation, is not really significant in comparison to the general noise in the signal. However, scanning with a better resolution just around resonance yields the signal presented in figure 3.13, revealing clearly the wrinkle. There is certainly no doubt that we observe some kind of saturated behaviour in the NICE-OHMS signal.

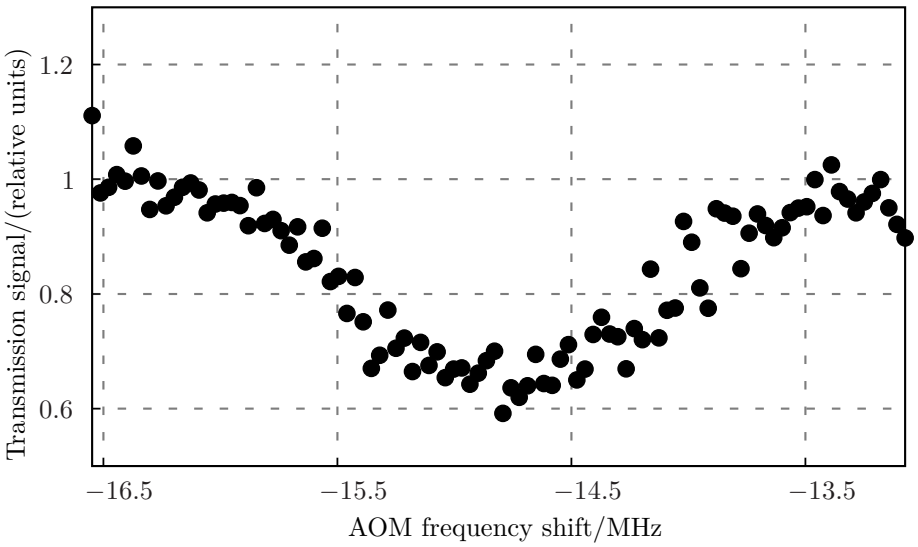

Figure 3.11: Cavity transmission. A broad scan of frequencies. The values on the x-axis is the frequency shift, imposed on the ULE cavity stabilized frequency, by an AOM (c.f., figure 1.3).

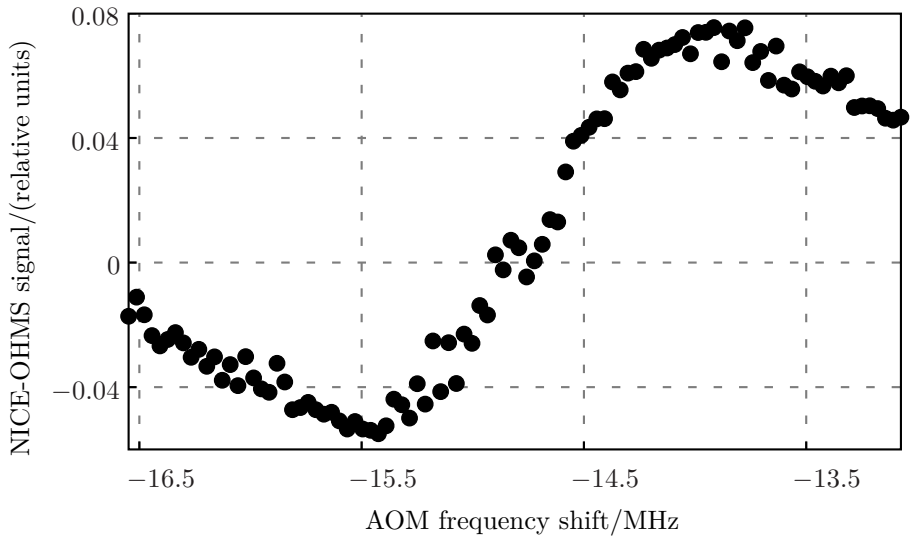

Figure 3.12: NICE-OHMS signal. A broad scan of frequencies. The values on the x-axis is the frequency shift, imposed on the ULE cavity stabilized frequency, by an AOM (c.f., figure 1.3).

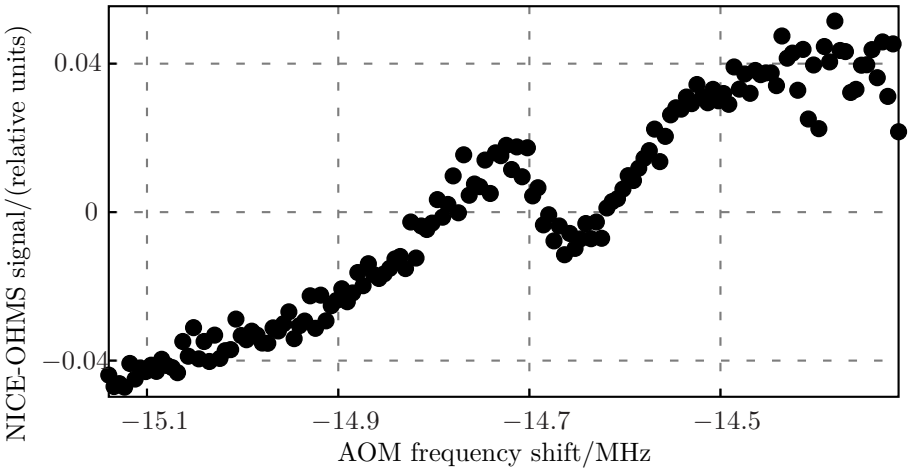

Figure 3.13: NICE-OHMS signal. A narrow scan of frequencies. The values on the x-axis is the frequency shift, imposed on the ULE cavity stabilized frequency, by an AOM (c.f., figure 1.3).

4 Conclusion

4.1 What Have We Learned

We have outlined the basic principles of an optical atomic clock, and motivated the investigation of the cavity-atom system as a mean of stabilizing the local oscillator of such a clock.

We have explained the principles of laser cooling and trapping, and delved in some of the considerations prior to constructing the trapping system. It has been showed that we are able to successfully load a MOT, thus realizing the cavity-atom system.

The theory and experimental methods necessary for measuring the phase shift of the probe beam, due to the atoms, has beam explained.

We have begun the analysis of the data produced by the setup. In a simple model, the overall shape of the NICE-OHMS signal is explained, but is is also clear that in order to use this signal as an error signal a more detailed analysis is necessary. I.e., we need to know which parameters must be tweaked in order to increase the slope of the signal around resonance.

4.2 Outlook: Continuous Error Signal Generation

The natural next experimental stage in the process of developing this new laser stabilization scheme, is to build a setup, that does not have to load and release the atoms, in order to make one measurement. For this to work as a stabilizing mechanism, we need continuous error signal feedback to the laser. Thus we are at this moment in the process of building an arrangement, that continuously probes a stream of cold, unperturbed atoms. At the same time, the arrangement described in this thesis is soon to be upgraded, by placing the cavity mirrors inside the vacuum chamber, instead of outside the windows. This way we will, hopefully, be able to eliminate thermal and acoustic noise to an even higher degree, thus getting even more precise data, and getting to understand the cavity-atom system even better.

4.3 Acknowledgements

I would like to thank my supervisor Jan W. Thomsen, Bjarke Christiansen, and Rastin Matin, for taking their time to introduce me to the experimental setup and the theoretical background, in a nice and easy way. I feel that I have learned incredibly much, in these 9 weeks.

Also i would like to thank Stefan Petersen, Martin Henriksen, Stefan Rathmann, and Asbjørn Jørgensen for making the time in the laboratory a great experience in a friendly and serious atmosphere.

Appendices

A Computing Theoretical B-field

```
clf; clc; clear all;
% Constants:
muB     = 9.27400968E-24;
Isat    = pi*6.6260E-34/3*2.998E8/(460.73E-9)^3*2.01E8; % = 427.5316
m       = 87.9*1.660538921E-27;
hbar    = 1.05457173E-34;
k       = 2*pi/(460.73E-9);
A       = 2.01E8;
% Parameters:
epsilon = 0.4;
P       = 32E-3;
w_i     = 0.001;
w_o     = 0.008;
L       = 0.3;
delta0  = -3.5E09;
M_J     = -1;
v_i     = 410;
% Initial conditions:
z(1)    = 0;
v(1)    = v_i;
s0      = 2*P./(pi*w_i.^2*Isat);
a(1)    = -epsilon*hbar*k*A/(m*2)*s0./(1+s0);
t(1)    = 0;
% Time steps:
dt      = 0.00000001;
% Computing v(z):
i       = 1;
while z(i)<0.3 && v(i)>0
    i   = i + 1;
    w   = w_i+z(i-1)/L*(w_o-w_i);
    s0  = 2*P./(pi*w.^2*Isat);
    a(i)= -epsilon*hbar*k*A/(m*2)*s0./(1+s0);
    v(i)= v(i-1) + a(i-1)*dt;
    z(i)= z(i-1) + v(i-1)*dt;
    t(i)= t(i-1) + dt;
end
disp('Exit velocity: '); disp(v(i));
% Computing B(z)
w   = w_i+z/L*(w_o-w_i);
s0  = 2*P./(pi*w.^2*Isat);
B   = hbar/(muB*M_J)*(A/2*sqrt((1+s0)*(1-epsilon)/epsilon) + k*v+delta0);
plot([-0.05 0 z 0.3 0.35],[0 0 B 0 0]);
```

B Simulating Phase-space Trajectories

```
clf; clc; clear z v;
% p is polynomial fitted to experimentally measured B-field
% Constants:
muB     = 9.27400968E-24;
Isat    = 425;
m       = 87.9*1.660538921E-27;
hbar    = 1.05457173E-34;
k       = 2*pi/(461E-9);
A       = 2.0E8;
% Parameters:
P       = 14E-3; % E.g.: 10, 14, 20, 22
w_i     = 0.001;
w_o     = 0.008;
delta0  = -3.5E09;
M_J     = -1;
L       = 0.3;
% Time steps:
dt      = 0.000001;
hold on;
for j = 30:30:580
    v(1)    = j;
    z(1)    = -0.027;
    i  = 1;
     while z(i)<0.316 && z(i)>=-0.027
         i = i + 1;
         B = polyval(p,z(i-1));
         w   = w_i+z(i-1)/L*(w_o-w_i);
         s0  = 2*P./(pi*w^2*Isat);
         delta = delta0 + k*v(i-1) - muB/hbar*B*M_J;
         a = -hbar*k/m*A/2*s0/(1+s0+(2*delta/A)^2);
         v(i) = v(i-1) + a*dt;
         z(i) = z(i-1) + v(i)*dt;
     end
    plot(z,v);
    clear z v;
end
axis([-0.027 0.316 0 600])
plot([-0.04 0.34],[30 30],'--k')
```

C Solving the Optical Bloch Equations

```
function RK4
% Constants
A    = 4.69E4;  % Decay rate of transition
% Parameters
Omega= 30E4;    % Rabi frequency
delta= 0;       % Detuning
% Initial conditions:
u(1) = 0;       % No dipole moment
v(1) = 0;       % No dipole moment
w(1) = 1;       % All atoms in ground state
t(1) = 0;
% Time steps:
dt   = 1/100000000;
% Computing u, v, and w:
tEnd = 200e-6;
for i = 2:tEnd/dt
    vk1 = dvdt(u(i-1),v(i-1),w(i-1),Omega,delta,A);
    wk1 = dwdt(v(i-1),w(i-1),A,Omega);
    uk1 = dudt(u(i-1),v(i-1),delta,A);

    vk2 = dvdt(u(i-1)+dt/2*uk1,v(i-1)+dt/2*vk1,w(i-1)+dt/2*wk1,Omega,delta,A);
    wk2 = dwdt(v(i-1)+dt/2*vk1,w(i-1)+dt/2*wk1,A,Omega);
    uk2 = dudt(u(i-1)+dt/2*uk1,v(i-1)+dt/2*vk1,delta,A);

    vk3 = dvdt(u(i-1)+dt/2*uk2,v(i-1)+dt/2*vk2,w(i-1)+dt/2*wk2,Omega,delta,A);
    wk3 = dwdt(v(i-1)+dt/2*vk2,w(i-1)+dt/2*wk2,A,Omega);
    uk3 = dudt(u(i-1)+dt/2*uk2,v(i-1)+dt/2*vk2,delta,A);

    vk4 = dvdt(u(i-1)+dt*uk3,v(i-1)+dt*vk3,w(i-1)+dt*wk3,Omega,delta,A);
    wk4 = dwdt(v(i-1)+dt*vk3,w(i-1)+dt*wk3,A,Omega);
    uk4 = dudt(u(i-1)+dt*uk3,v(i-1)+dt*vk3,delta,A);

    w(i) = w(i-1) + dt/6*(wk1 + 2*wk2 + 2*wk3 + wk4);
    v(i) = v(i-1) + dt/6*(vk1 + 2*vk2 + 2*vk3 + vk4);
    u(i) = u(i-1) + dt/6*(uk1 + 2*uk2 + 2*uk3 + uk4);

    t(i) = t(i-1) + dt;
end
clf; hold on;
plot(t,u,'r');
plot(t,v,'g');
plot(t,w,'b');
```

```
end
% Optical Bloch equations:
function uDot = dudt(u,v,Delta,A)
   uDot = Delta*v - A/2*u;
end
function vDot = dvdt(u,v,w,Omega,Delta,A)
   vDot = -Delta*u + Omega*w - A/2*v;
end
function wDot = dwdt(v,w,A,Omega)
   wDot = -Omega*v-A*(w-1);
end
```

Bibliography

[1] Riehle, F., "Frequency Standards, Basics and Applications",
Wiley, (2004).

[2] NIST Historical context of the SI,
http://physics.nist.gov/cuu/Units/second.html, (March 1st 2014).

[3] Le Targat, R. et al., "Experimental realization of an optical second with strontium lattice clocks",
Nature Communications **4**, 2109, (2013).

[4] Bloom, B. J. et al., "An optical lattice clock with accuracy and stability at the 10^{-18} level",
Nature **506**, 71-75, (2014).

[5] Martin, M. J. et al., "Extreme nonlinear response of ultranarrow optical transitions in cavity QED for laser stabilization",
Phys. Rev. A **84**, 063813, (2011).

[6] NIST Atomic Spectra Database Lines,
http://physics.nist.gov/PhysRefData/ASD/lines_form.html, (March 1st 2014).

[7] Ye J. et al., "Cooling and trapping of atomic strontium",
J. Opt. Soc. Am. B **20**, 968-976, (2003).

[8] Matin, R., "Towards Continuous Cavity-Enhanced Nonlinear Spectroscopy in Strontium",
University of Copenhagen, (2013).

[9] Foot, C. J., "Atomic Physics",
Oxford University Press, (2012).

[10] Eberly, J. H., Milonni, P. W., "Laser Physics",
Wiley, (2010).

[11] Vuletic V. et al., "Interaction between Atomic Ensembles and Optical Resonators: Classical Description",
Elsevier, (2011).

[12] Hänsch T. W, Couillaud, B., "Laser frequency stabilization by polarization spectroscopy of a reflecting reference cavity",
Optics Communication **35**, 441-444, (1980).

[13] Cerea A., "NICE-OHM Spectroscopy of $|^1S_0\rangle \rightarrow |^3P_1\rangle$ transition in ^{88}Sr atoms",
University of Copenhagen, (2013).